Experimental investigation of non-monotonic fracture conductivity evolution in energy georeservoirs

Zihao Li [a,b], Qingqi Zhao [c], Yuntian Teng [c], Ming Fan [a], Nino Ripepi [a], Xiaolong Yin [d], Cheng Chen [c,*]

[a] Department of Mining and Minerals Engineering, Virginia Tech, Blacksburg, VA, 24061, USA
[b] Now at School of Civil and Environmental Engineering, Cornell University, Ithaca, NY, 14853, USA
[c] Department of Civil, Environmental and Ocean Engineering, Stevens Institute of Technology, Hoboken, NJ, 07030, USA
[d] Petroleum Engineering Department, Colorado School of Mines, Golden, CO, 80401, USA

ARTICLE INFO

ABSTRACT

Significant fracture conductivity can be achieved using a much lower material cost based on the optimal partial-monolayer proppant concentration (OPPC) theory. However, experimental validation and investigation of the OPPC theory have been extremely rare in the literature. In this study, we used a laboratory fracture conductivity cell to conduct well-controlled fracture conductivity experiments to comprehensively study the role of effective stress, proppant size, rock type, and water soaking on the evolution of fracture conductivity as a function of increasing proppant concentration. With seven proppant concentrations (up to 2 lb/ft^2) and seven effective stresses (up to 6000 psi) used in the conductivity measurements, we experimentally confirmed that the correlation between fracture conductivity and proppant concentration was non-monotonic because of a competing process between fracture permeability and fracture width. We also investigated the influence of the above-mentioned experimental conditions on the OPPC and the corresponding optimal fracture conductivity (OFC). This is the first study that uses well-controlled laboratory experiments to comprehensively investigate non-monotonic fracture conductivity evolutions. The existence of the OPPC indicates that a relatively low proppant amount can be used to form a partial-monolayer proppant pack in the fracture space, which has similar or higher fracture conductivity compared to a multilayer proppant structure. This finding has important economic implications because high-strength, ultralight-weight proppant particles can be used to form partial-monolayer proppant packs in fractures, leading to sufficiently high fracture conductivity using a much lower material cost compared to multilayer proppant structures. Our experiments illustrated that proppant embedment is the primary mechanism that causes the competing process between fracture width and fracture permeability and consequently the non-monotonic fracture conductivity evolution as a function of increasing proppant concentration. Without proppant embedment, there will not be such a competing process, and the non-monotonic fracture conductivity evolution will not be observed.

1. Introduction

Unconventional hydrocarbon reservoirs, including shale, tight sandstone, and oil-sand, contain massive amounts of fossil energy, but they present tremendous technical challenges to both geoscientists and engineers in terms of recovering these energy resources at an economically viable rate (Gensterblum et al., 2015; Wang et al., 2018; Hu et al., 2021). Multiple enhanced production technologies have been implemented to achieve economical production rates from these tight

reservoirs (Li et al., 2016, 2019; Tan et al., 2020). Hydraulic fracturing is an enhanced oil/gas recovery process that is commonly used in extremely low permeability rocks to promote oil and/or gas flow. It typically involves the injection of high-pressure water and sand into a bedrock formation through the wellbore (Montgomery and Smith, 2010; Tillman et al., 2015; Li et al., 2020; 2021; Zhao et al., 2021). The hydraulically-created fractures may close during production as a result of reduced fluid pressure and increased effective stress in the fractures (Fan et al., 2019). Therefore, it is critical that proppant slurries are

pumped into the induced fractures or existing fractures to increase the size and extent of the fractures and to provide long-term fracture productivity (Liang et al., 2016).

Fracture conductivity, defined as the product of fracture permeability and fracture width (Chen et al., 2015), measures the fluid flow rate through a unit length of fracture and thus is directly related to the productivity of the fracture. A sufficiently high fracture conductivity is essential for the extraction of hydrocarbons at an economically viable rate. Fracture width and permeability are closely related to the number of proppant particles placed in the fracture and the effective stress imposed on the proppant pack (Chen et al., 2015; Fan et al., 2019). A proppant mixture with different particle sizes is usually injected into the wellbore during the hydraulic fracturing process. Typically, a smaller-sized proppant is injected first, followed by a larger-sized proppant. The amount of proppant placed in a fracture is measured by proppant concentration, also known as proppant areal concentration, which is defined as the proppant mass per unit of fracture surface area, usually in pounds per square foot (lb/ft^2) (Economides and Nolte, 2000).

The conventional method of increasing fracture conductivity is to inject a large amount of proppant particles to form a multilayer proppant structure, which enhances the fracture width. However, the material cost can be a potential issue associated with multilayer proppant structures. Some man-made ceramic proppant is relatively expensive, especially the ultra-lightweight (ULW) proppant, and the price can range from $5/lb to $10/lb (Gu et al., 2015). In the scenarios where expensive ceramic proppant is needed, it has great economic benefits to use a lower proppant concentration in hydraulic fractures. According to the definition of fracture conductivity, it is critical to consider both fracture width and fracture permeability in order to achieve the highest fracture conductivity. Previous studies in the literature showed that effective stress, proppant compaction, and proppant embedment all have a significant impact on fracture conductivity (McGinley et al., 2015; Zhang et al., 2016; Mittal et al., 2018; Zheng et al., 2018; Fan et al., 2021). Many numerical modeling studies have also been conducted to investigate the influence of proppant compaction and embedment on fracture conductivity (Zhang et al., 2017; Fan et al.,

Table 1
Comprehensive literature review of relevant studies on fracture conductivity and proppant concentrations.

Studies	Methods	Range of proppant concentration	Non-monotonic behavior	Discussion of Embedment	Role of rock type	Role of proppant size	Role of water soaking	Role of effective stress
This work	Laboratory experiment	Partial-monolayer, monolayer, and multilayer	Yes	Yes	Berea sandstone, Marcellus shale	20/40 and 40/70 ceramic proppants	Yes	500, 1000, 2000, 3000, 4000, 5000, and 6000 psi
Brannon et al. (2004)	Laboratory experiment	Partial-monolayer and multilayer	Yes	No	Ohio sandstone	20/40, 12/20, and 8/16 Brady sands and 20/40 ULW proppants	No	1000, 2000, 4000, and 6000 psi
Weaver et al. (2009)	Laboratory experiment	N/A	No	No	Shale, sandstone	Four synthetic proppants	Yes	4000, 8000, 12,000, and 16,000 psi
Gaurav et al. (2012)	Laboratory experiment	Monolayer, multilayer	No	No	Steel shim, Barnett shale	18/40, 16/35, and 14/25 ULW proppants	No	1000, 2000, 4000, and 6000 psi
(Kunnath Aven et al., 2013)	Laboratory experiment	N/A	No	No	N/A	20/40 silica-based and ceramic proppants	Yes	N/A
Raysoni and Weaver (2013)	Laboratory experiment	N/A	No	No	Low-permeability sandstone	20/40 aluminum-based proppant	Yes	N/A
McGinley et al. (2015)	Laboratory experiment	Partial-monolayer, monolayer	No	No	Marcellus shale	40/70 natural white sand	No	1000, 2000, 3000, 4000, 5000, and 6000 psi
Zhang et al. (2016)	Laboratory experiment	Partial-monolayer, monolayer	No	Yes	Barnett shale, Eagle Ford shale, Berea sandstone	40/70 and 30/50 Badger sands	Yes	4000 and 6000 psi
Bestaoui-Spurr and Hudson (2017)	Laboratory experiment	Partial-monolayer	No	No	Ohio sandstone	14/40 ULW proppant	No	1000, 3000, 5000, 6000, 7000, 8000, 9000, and 10,000 psi
Zhang et al. (2017)	Numerical simulation and laboratory experiment	Multilayer	No	Yes	Longmaxi shale	20/40, 30/50, 40/70 ceramic proppants	No	2 MPa (290 psi) and 30 MPa (4351 psi)
Mittal et al. (2018)	Laboratory experiment	Multilayer	No	Yes	Vaca Muerta shale, Eagle Ford shale, metal	20/40, 40/70, and 60/100 Ottawa sands	Yes	5000 psi
Zheng et al. (2018)	Laboratory experiment	Multilayer	No	No	N/A	20/40 and 30/50 ceramic proppants, 20/40 coated sand	No	2–30 MPa (290–4351 psi)
Fan et al. (2019)	LB modeling	Partial-monolayer, monolayer, multilayer	Yes	Yes	Sandstone	0.63, 0.45, and 0.32 mm	No	1000, 2000, 4000, 6000 psi
Bhandakkar et al. (2020)	Numerical simulation	N/A	No	No	N/A	0.0065, 0.01, and 0.02 inch	No	N/A
Fan et al. (2021)	LB modeling and laboratory experiment	Monolayer, multilayer	No	Yes	Berea sandstone, Eagle Ford shale	20/40 ceramic proppant and sand	Yes	1000, 2000, 4000, 6000 psi

"N/A" denotes "not available".

2019; Bhandakkar et al., 2020).

Previous studies have shown that a partial-monolayer proppant structure can achieve significant fracture conductivity because the high porosity of the fracture space leads to high fracture permeability (Brannon et al., 2004; Weaver et al., 2009; Kunnath Aven et al., 2013; Raysoni and Weaver, 2013). This has significant economic implications because a partial-monolayer proppant structure results in a lower material cost. Table 1 provides a comprehensive literature review for relevant studies on fracture conductivity and proppant concentrations. It is clear that this study is the first to use well-controlled, comprehensive laboratory experiments to study the role of different rock types (i.e., both conventional and unconventional reservoir rocks) and water soaking on non-monotonic fracture conductivity evolutions. In addition, this study provides in-depth discussions on the role of proppant embedment on rock surfaces, which is the fundamental mechanism that causes non-monotonic fracture conductivity evolution as a function of increasing proppant concentration. Particularly, the experimental data from this work provides direct laboratory evidence to support the theory developed in our previous study (Fan et al., 2019), which used numerical modeling to illustrate that proppant embedment is the primary mechanism that causes the competing process between fracture width and fracture permeability and consequently the non-monotonic fracture conductivity evolution behavior.

This study conducted well-controlled, comprehensive laboratory experiments to measure fracture conductivity as a function of proppant concentration ranging from 0 lb/ft^2 to 2 lb/ft^2, which accounts for the transition from a partial-monolayer proppant assembly structure to a multilayer proppant assembly structure. This work is the first study that uses well-controlled laboratory experiments to comprehensively investigate non-monotonic fracture conductivity evolution as a function of increasing proppant concentration under various effective stresses, proppant particle sizes, rock types, and water soaking time. The findings from this experimental study will advance the fundamental understanding of proppant embedment and compaction and will contribute to the development of workflows for optimizing proppant placement and maximizing productivity in hydraulic fracturing.

2. Theory of optimal partial-monolayer proppant concentration

Because a partial-monolayer proppant structure has high porosity, which leads to high fracture permeability, it is possible to increase the overall fracture conductivity by decreasing the proppant concentration from a multilayer proppant pack to a partial-monolayer proppant pack (Huitt and Mcglothlin, 1958; Darin and Huitt, 1960). Although the optimal partial-monolayer proppant concentration theory was developed decades ago, the field applications had not been possible until the development of slickwater and ULW proppant in hydraulic fracturing (Brannon et al., 2004). Previous experimental studies showed that partial-monolayer proppant assemblies provided higher or equivalent fracture conductivity compared to conventional multilayer proppant assemblies (Brannon et al., 2004; Gaurav et al., 2012; Bestaoui-Spurr and Hudson, 2017). Parker et al. (2012) demonstrated in field testing that a lightweight thermoplastic alloy proppant could form a partial-monolayer structure and increase the production rate. Our recent study (Fan et al., 2019) was the first one to elucidate the multiphysics processes that lead to non-monotonic fracture conductivity evolution, which is caused by non-monotonic fracture permeability evolution and a competing process between fracture permeability and fracture width. Specifically, Fan et al. (2019) combined laboratory penetrometer experiments with the discrete element method (DEM) and lattice Boltzmann (LB) method to track the detailed evolutions of fracture permeability and fracture width when the proppant pack developed from a partial-monolayer structure to a multilayer structure; the result validated the theory that explained why non-monotonic fracture conductivity evolution occurs, which will be described below.

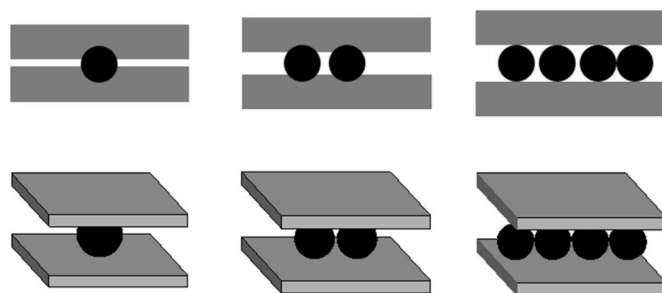Fig. 1 illustrates proppant embedment mitigation in a fracture with

Fig. 1. Front view (top row) and 3D view (bottom row) of the mitigation of proppant embedment in a fracture with an increasing proppant concentration (i.e., from left to right). This picture was modified from Fan et al. (2019).

an increasing proppant concentration. Proppant crushing is not considered in this case because some ceramic proppant can withstand external stresses up to 10,000 psi (Liang et al., 2016). The detailed evolutions of fracture width, porosity, permeability, and conductivity go through four distinct stages with the increasing proppant concentration, which are demonstrated in Table 2.

Stage 1: Because of the low proppant concentration in this stage, proppant embedment is significant at the beginning. The increasing number of proppant particles entering the fracture space significantly mitigates proppant embedment, thereby increasing the fracture width and fracture permeability. However, on the other hand, the increasing proppant particles occupy the empty fracture space, leading to reduced fracture porosity, which has a negative effect on fracture permeability. Because the permeability increase resulting from fracture width increase surpasses the permeability loss resulting from fracture porosity reduction, the net effect is that fracture permeability increases, which results in increasing fracture conductivity because both fracture permeability and width increase in this stage.

Stage 2: With continuously increasing proppant particles placed in the fracture space, the permeability loss resulting from fracture porosity reduction surpasses the permeability gain resulting from fracture width increase, leading to decreased fracture permeability. However, when fracture permeability begins to decline, its reduction rate is slower than the rate of fracture width increase. Therefore, the fracture conductivity, which is the product of fracture permeability and fracture width, still increases in this stage.

Stage 3: When the rate of permeability reduction surpasses the rate of fracture width increase with increasing proppant particles in the fracture, fracture conductivity reaches the local maximum and then starts to decline. The proppant concentration corresponding to the local maximum fracture conductivity is referred to as the optimal partial-monolayer proppant concentration (OPPC), and the local maximum fracture conductivity is referred to as the optimal fracture

Table 2

Evolutions of fracture width, w_f, porosity, φ, permeability, k, and conductivity, $k \cdot w_f$, with an increasing proppant concentration.

	w_f	φ	k	Fracture conductivity ($k \cdot w_f$)	Geometry of proppant pack
Stage 1	↑	↓	↑	↑	Partial monolayer
Stage 2	↑	↓	↓	↑	Partial monolayer
Stage 3	↑	↓	↓	↓	Partial monolayer to monolayer
Stage 4	↑	→	→	↑	Monolayer to multilayer

Note: The arrows "↑", "↓", and "→" denote "increase", "decrease", and "stay constant", respectively. This table was modified from Fan et al. (2019).

conductivity (OFC). Stage 3 continues developing until the proppant particles cover the entire rock surface, lead to a full-monolayer proppant pack.

Stage 4: In this stage, the proppant pack develops from a full-monolayer structure to a multilayer structure. Because the proppant assembly has become a fully-packed porous medium, its porosity and permeability are dominated primarily by the average grain and pore sizes and insensitive to the fracture width (Chen et al., 2008, 2009). Therefore, fracture permeability and porosity in Stage 4 will not vary significantly with increasing proppant particles placed in the fracture.

Fan et al. (2019) combined laboratory penetrometer experiments with DEM/LB numerical modeling to demonstrate non-monotonic fracture conductivity evolutions when the proppant assembly developed through the above-mentioned four stages, as shown in Fig. 2. Particularly, three particle sizes (0.63 mm, 0.45 mm, and 0.32 mm) and four effective stresses (1,000, 2,000, 4,000, and 6000 psi) were considered, resulting in twelve curves. Fig. 2 illustrates the role of proppant particle size and effective stress on the OFC and OPPC, and the fracture conductivity values in this plot was numerically simulated using the LB method. When particle size stayed constant, the OFC declined with increasing effective stress because of the reduced fracture permeability and width under higher effective stress. In addition, the OPPC increased (i.e., was shifted to the right) with increasing effective stress because keeping the fracture open under higher effective stress required more proppant particles. When the effective stress was sufficiently high, the OPPC approached the full-monolayer proppant concentration because in this case a partial-monolayer proppant structure was unable to keep the fracture open. When the effective stress stayed constant, the proppant assembly with 0.63 mm particle diameter had the maximum OFC, and the proppant assembly with 0.32 mm particle diameter had the minimum OFC. This was because a partial-monolayer proppant assembly having larger particle diameter led to larger fracture permeability and width. Fan et al. (2019) obtained these findings using an experiment/simulation-integrated workflow. The objective of this paper is to conduct well-controlled laboratory experiments to study the role of effective stress, proppant particle size, water soaking, and rock type on the evolution of fracture conductivity as a function of increasing proppant concentration.
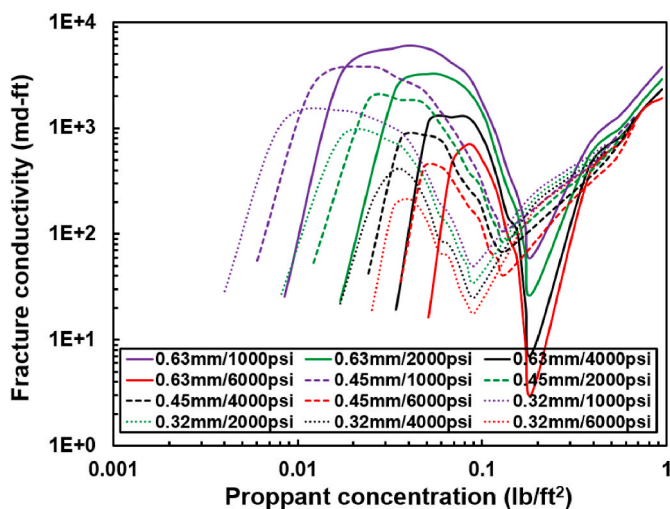
3. Laboratory equipment, materials, and workflow

Fig. 3 illustrates the schematic plot and laboratory photo of the fracture conductivity cell used in the experiments, which can measure fracture conductivity under different closure pressures and temperatures. In the test, two rock slabs and proppant particles sandwiched between them are placed in the testing cell, which is subjected to a closure pressure up to 17,000 psi with a precision of 0.2%. An electrical heater provides a testing temperature up to 250 °C with a precision of 0.4%. The proppant concentration in the fracture was measured using the proppant mass and the surface area of the rock slabs. The fracture conductivity, C, according to the API RP-19D standard (2008), is the flow rate contributed by a unit length of fracture and calculated as:

$$C = kw_f = \frac{\mu \cdot Q \cdot L \cdot w_f}{\Delta p \cdot A} = \frac{\mu \cdot Q \cdot L}{\Delta p \cdot h} \qquad (1)$$

where C is fracture conductivity (m^3); k is fracture permeability (m^2); w_f is fracture width (m); h is the size of the longer dimension of the fracture cross section (m); A is the area of fracture cross section and equal to $w_f h$ (m^2); μ is fluid viscosity (Pa·s); Q is flow rate (m^3/s); L is the length over which the pressure difference is measured (m); Δp is the pressure difference (Pa). Note that μ, L, and h in Equation (1) are known. The measured flow rate, Q, and pressure difference, Δp, are then imported into Equation (1) to calculate the fracture conductivity.

Fig. 4 illustrates the diameter distributions of the two ceramic proppants used in the experiments. Particularly, the mesh-20/40 proppant had particle diameters in the range between 400 μm and 841 μm. The mesh-40/70 proppant had particle diameters in the range between 210 μm and 400 μm. We used Berea sandstone and Marcellus shale as the rock slabs in the testing. Each rock slab was of 7 inches in length, 1.5 inches in width, and 0.5 inch in thickness. Table 3 and Table 4 illustrate the properties of the sandstone slabs and shale slabs, respectively. All the rock slabs had flat surfaces and their initial roughness values were the same. In addition, the rock slabs had the same initial hardness because they were cored from the same chunks of rock materials.

Seven proppant concentrations (0, 0.02, 0.06, 0.1, 0.2, 1, and 2 lb/ft^2) and seven effective stresses (500, 1000, 2000, 3000, 4000, 5000, and 6000 psi) were used in the conductivity measurement experiments, leading to 49 conductivity measurements in each plot. We conducted these measurements on four different combinations of rock and proppant: (1) Berea sandstone + mesh-20/40 ceramic proppant, (2) Berea sandstone with 30 days of water soaking + mesh-20/40 ceramic proppant, (3) Berea sandstone + mesh-40/70 ceramic proppant, and (4) Marcellus shale + mesh-20/40 ceramic proppant. These comprehensive measurements aimed to study the role of proppant concentration, rock type, water soaking, and proppant size on fracture conductivity under increasing effective stresses. Detailed experimental conditions in this study are listed in Table 1.

4. Results and discussion

Fig. 5 demonstrates that overall the proppant fracture conductivity decreased with an increasing effective stress because of the proppant embedment into rock surfaces. In addition, it was observed that the fracture conductivity measured on the sandstone slabs did not change noticeably when the effective stress was higher than 5000 psi. In comparison, the fracture conductivity measured on the shale slabs did not change noticeably when the effective stress was higher than 3000 psi. This was because proppant embedment did not develop noticeably when the effective stress was sufficiently high, leading to a relatively steady proppant structure in the fracture under high stresses. In these experiments, a particular proppant concentration was placed in the fracture space between two rock slabs, and then the rock slabs were pushed toward each other to increase the effective stress stepwise to measure the fracture conductivity values under seven stress levels (i.e., 500, 1000,

Fig. 2. Role of proppant particle size and effective stress on the fracture conductivity versus proppant concentration curve, which was based on LB numerical simulation. This picture is from Fan et al. (2019).
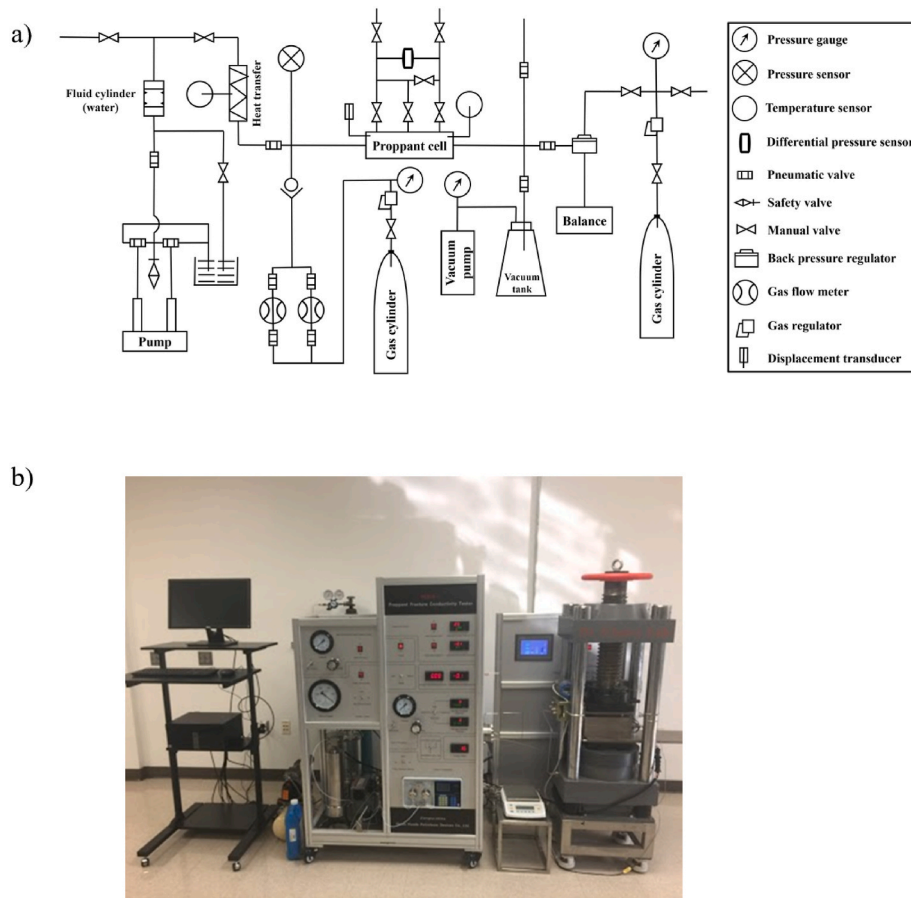
Fig. 3. a) Schematic plot, and b) laboratory picture of the fracture conductivity cell used in this study. The schematic plot was provided by the manufacturer.
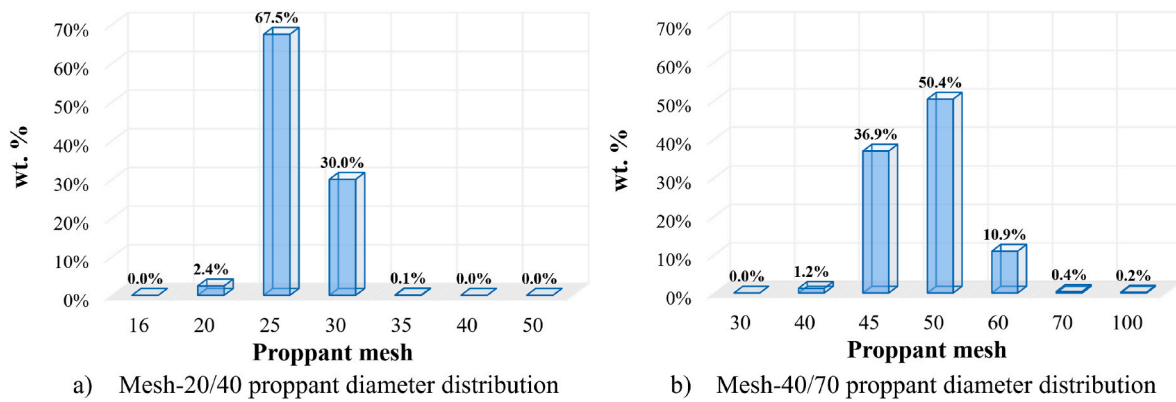

a)   Mesh-20/40 proppant diameter distribution   b)   Mesh-40/70 proppant diameter distribution

Fig. 4. Diameter distributions of ceramic proppant having a mesh size of a) 20/40, and b) 40/70 used in the fracture conductivity measurements.

Table 3
Geomechanical properties of the Berea sandstone used in the experiments (data from Kocurek Industries, Inc.).

Test Results	Rock Strength (MPa)	Ultrasonic Wave Velocity (ft/s)		Density (g/cm³)	Dynamic Young's Modulus (GPa)	Dynamic Poisson's Ratio	Grain Size (μm)	Perm. (mD)	FTIR Mineralogy (%)		
		V_p	V_s						Quartz	Kaolinite	Montmorillonite
Mean	56	8319	5695	2.3	14.4	0.06	122.3	4.4	91	8	1
STD	6	357	217				10.2	2.7			
Min	42	8035	5501				108.1	1.4			
Max	66	8752	5942				139.3	9.8			

Table 4
Mineralogy of Marcellus shale used in the experiments (data from Kocurek Industries, Inc.).

TOC Wt.%	Carbonate Wt. %	Tmax (C)	Calculated Ro	Quartz	Clay	Illite/Semctite
4.45	40	0	0	45.9	15.3	–
Feldspar	Pyrite	Calcite	Kaolinite	Dolomite	Microcline	Albite
–	2.8	26.6	1.2	4.0	1.4	2.8
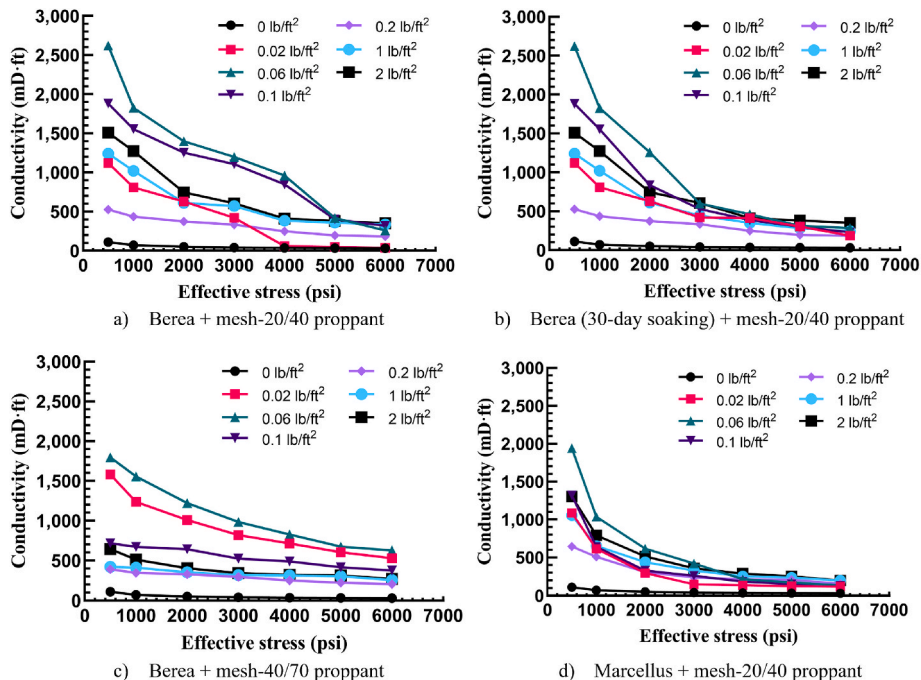
Fig. 5. Measured fracture conductivity as a function of effective stress for a) Berea + mesh-20/40 proppant, b) Berea (30-day water soaking) + mesh-20/40 proppant, c) Berea + mesh-40/70 proppant, and d) Marcellus + mesh-20/40 proppant.

2000, 3000, 4000, 5000, and 6000 psi). At the end of the test (i.e., after the 6000 psi test), significant proppant embedment and development of microscale fractures on rock surfaces were observed. Thus, the rock slabs cannot be reused after the 6000 psi test, and another pair of intact rock slabs were used for the test with a different proppant concentration. Therefore, seven pairs of rock slabs were used in each plot shown in Fig. 5 because we conducted the experiments under seven different proppant concentrations (i.e., 0, 0.02, 0.06, 0.1, 0.2, 1, and 2 lb/ft^2). It is interesting to observe that the fracture conductivity for 0.02 lb/ft^2 in Fig. 5a suddenly approached zero when the effective stress was higher than 4000 psi. This was attributed to the bedding planes of weakness in this particular pair of Berea sandstone slabs, which led to the rapid development of microscale fractures on the rock surface when the effective stress rose to 4000 psi. These fractures on rock surface caused significant proppant embedment, which has been observed in our previous experimental study (Chen et al., 2015) that used high-resolution X-ray computed tomography scanning to investigate proppant particle embedment on rock surfaces.

Comparison between Fig. 5a and b suggests that the 30-day water soaking caused rock surface softening and clay swelling, which led to significant proppant embedment and consequently faster fracture conductivity decline under increasing effective stress. Comparison between Fig. 5a and c shows that proppant particle diameter impacted fracture conductivity noticeably. With the same proppant concentration and under the same effective stress, the fracture conductivity of proppant having larger diameter (i.e., mesh-20/40) was generally higher than that of the proppant having smaller diameter (i.e., mesh-40/70). This was because larger proppant particles provided larger average pore size in the proppant assembly structure, leading to higher fracture

permeability. In addition, comparisons between Fig. 5a and d indicate that fracture conductivity measured on the Berea sandstone slabs was noticeably higher than that measured on the Marcellus shale slabs under the same proppant concentration and effective stress. This was because the shale slabs had a higher clay content compared to the sandstone slabs, leading to larger proppant embedment depth and consequently lower fracture conductivity in the shale fracture.

Fig. 6 illustrates measured fracture conductivity as a function of proppant concentration. Non-monotonic fracture conductivity evolution can be clearly observed in all four plots as a function of increasing proppant concentration. This is the first study that uses well-controlled laboratory experiments to comprehensively investigate non-monotonic fracture conductivity evolution as a function of increasing proppant concentration under various effective stresses, proppant particle sizes, rock types, and water soaking time. The existence of the OPPC indicates that a relatively low proppant amount can be used to form a partial-monolayer proppant pack in the fracture space, which has similar or higher fracture conductivity compared to a multilayer proppant structure. Some field cases have been reported where partial-monolayer proppant packs were deployed successfully (Posey and Strickland, 2005; Dahl et al., 2015). This finding has important economic implications because high-strength, ultralight-weight proppant particles can be used to form partial-monolayer proppant packs in fractures, leading to sufficiently high fracture conductivity using a much lower material cost compared to multilayer proppant structures.

Fig. 6 shows that the OPPC value was around 0.06 lb/ft^2 for all the four groups of experiments, which was close to the value (i.e., 0.04 lb/ft^2) found in our previous study that was based on laboratory penetrometer experiments and DEM/LB modeling (Fan et al., 2019). Overall,
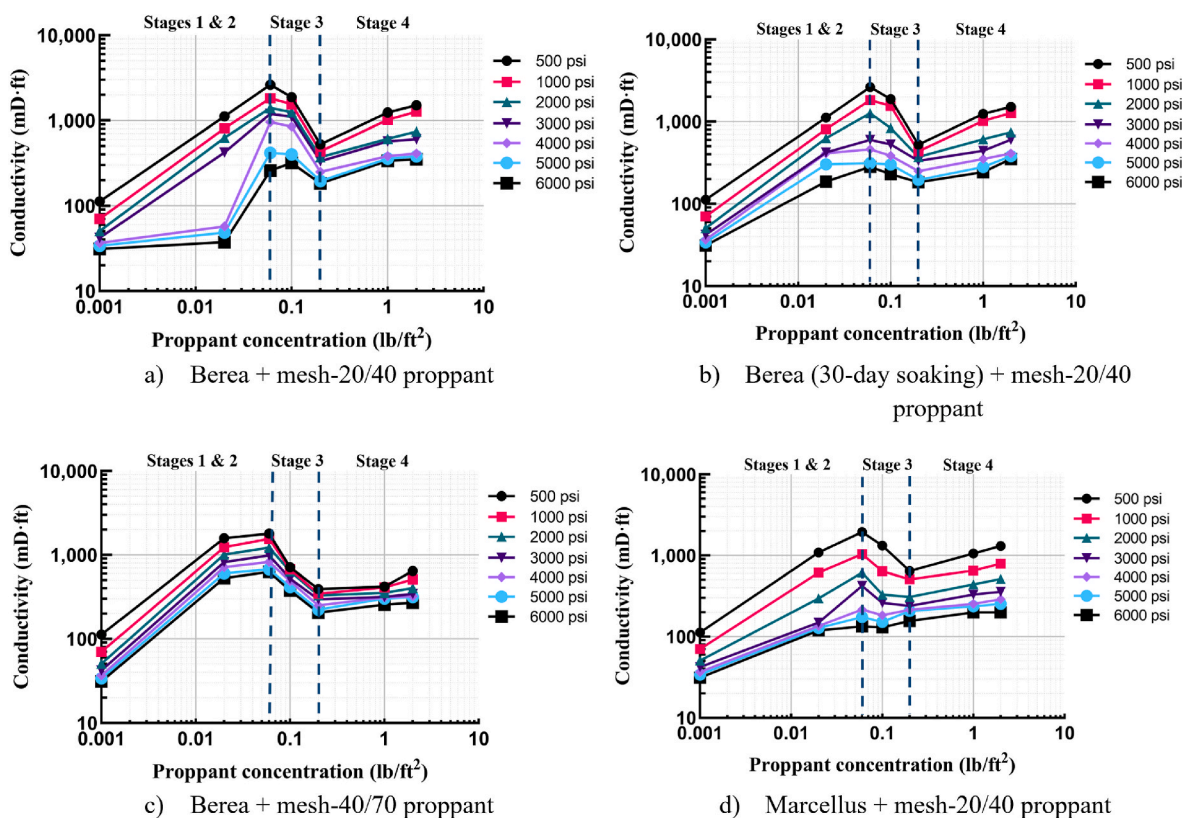
Fig. 6. Measured fracture conductivity as a function of proppant concentration for a) Berea + mesh-20/40 proppant, b) Berea (30-day water soaking) + mesh-20/40 proppant, c) Berea + mesh-40/70 proppant, and d) Marcellus + mesh-20/40 proppant. The two vertical dash lines divide the proppant concentration domain into three zones: Stages 1 and 2 (partial monolayer), Stage 3 (partial monolayer to full monolayer), and Stage 4 (full monolayer to multilayer), as described in Table 2.

the OFC decreased under increasing effective stress because a higher effective stress imposed on the proppant pack led to larger proppant embedment depth and tighter particle packing, which reduced both the fracture permeability and fracture width, thereby decreasing the fracture conductivity. Fig. 7 illustrates the measured OFC as a function of increasing effective stress for the four groups of experiments. Furthermore, the OPPC had the tendency to increase under an increasing effective stress. For example, the OPPC value in Fig. 6a (i.e., sandstone + mesh-20/40 proppant) shifted from 0.06 lb/ft^2 to 0.1 lb/ft^2 when the effective stress reached 6000 psi. This suggested that more proppant particles were required to open the fracture and to achieve the OFC under a higher effective stress. However, this tendency was observed only in Fig. 6a; the OPPC did not change in the other three groups of experiments. This implied that the effective stress had a more noticeable impact on the OFC than on the OPPC.
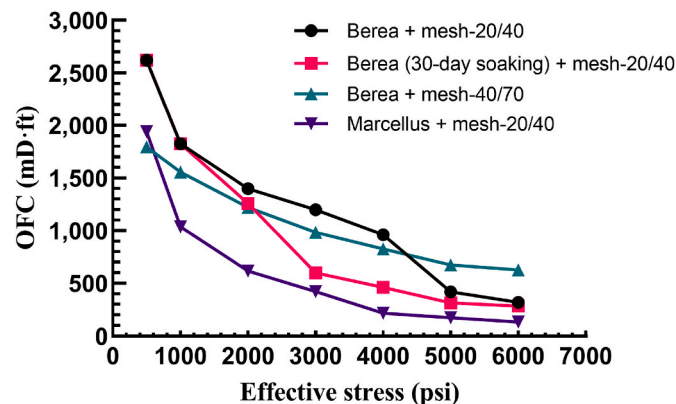

Fig. 7. Measured OFC as a function of effective stress.

Particularly, Fig. 6a shows that mesh-20/40 proppant sandwiched between two Berea sandstone slabs and subjected to an effective stress of 1000 psi led to an OPPC value of 0.06 lb/ft^2 and an OFC value around 2000 mD·ft. In comparison, our previous work (Fan et al., 2019) combined laboratory penetrometer experiments with DEM/LB numerical modeling to find that the OPPC and OFC values were 0.04 lb/ft^2 and 6000 mD·ft, respectively, for proppant having 0.63 mm dimeter that were sandwiched between two sandstone slabs and subjected to an effective stress of 1000 psi, as shown in Fig. 2. The differences between these two studies resulted from different proppant particle size distributions and rock surface roughness. In the previous study (Fan et al., 2019), the proppant particles had a homogeneous diameter equal to 0.63 mm, the average size of mesh-20 and mesh-40 particles. Conversely, in this experimental laboratory study, the mesh-20/40 proppant particles had a heterogeneous size distribution between mesh-40 and mesh-20 diameters as shown in Fig. 4. Therefore, in the laboratory experiments, smaller particles can fill in the pore space between larger particles, leading to lower fracture porosity and consequently lower fracture conductivity. In addition, the DEM/LB numerical modeling in our previous study (Fan et al., 2019) assumed smooth rock surfaces, which was favorable for fluid flow in the fracture. Conversely, in the laboratory experiments the Berea sandstone slabs had surface roughness, which negatively impacted the fracture permeability and consequently reduced the fracture conductivity. The rough rock surface and heterogeneous proppant size caused that the OFC measured in the laboratory (i.e., 2000 mD·ft) was lower than that measured using DEM/LB modeling (i.e., 6000 mD·ft). Furthermore, because proppant size was heterogeneous in the laboratory experiments, only the largest proppant particles were in contact with both rock surfaces in the partial-monolayer structure; the smaller particles were not in contact with both rock surfaces and thus were not responsible for keeping the fracture open. As a consequence, only a portion of the proppant particles

were subjected to effective stress, and thus more proppant particles were needed to achieve the same fracture conductivity. This explained why in the laboratory experiments the observed OPPC value (i.e., 0.06 lb/ft^2) was higher than that found by DEM/LB modeling (i.e., 0.04 lb/ft^2).

Fig. 8 and Fig. 9 illustrate the rock slab surfaces with proppant concentrations of 0.06 lb/ft^2 and 2 lb/ft^2, respectively, after experimental testing of 6000 psi. Particularly, proppant concentrations of 0.06 lb/ft^2 and 2 lb/ft^2 resulted in a partial-monolayer proppant assembly and multilayer proppant assembly in the fracture, respectively. It was observed that the embedment depth for the proppant concentration of 0.06 lb/ft^2 (i.e., the partial-monolayer structure) was larger than that for the proppant concentration of 2 lb/ft^2 (i.e., the multilayer structure). This was because the smaller amount of proppant particles in the partial-monolayer proppant structure led to higher mechanical loading imposed on each individual proppant particle, resulting in a larger embedment depth. This suggests that it is extremely important to account for the effect of proppant embedment on rock surfaces in a partial-monolayer proppant assembly. Proppant embedment is the primary mechanism that causes the competing process between fracture width and fracture permeability and consequently the non-monotonic fracture conductivity evolution, as shown in Table 2. Without proppant embedment, there will not be such a competing process, and we will not observe the non-monotonic fracture conductivity evolution in the laboratory.

Some numerical studies in the literature have investigated fracture conductivity provided by a partial-monolayer proppant structure based on the assumption that the proppant particles and rock surfaces are ideal, rigid materials, which means that proppant embedment on rock surfaces does not occur. Based on this no-embedment assumption, the simulated fracture conductivity decreased monotonically with an increasing proppant concentration when the proppant assembly is a partial-monolayer structure. In other words, the OPPC in this case is to place only one proppant particle in the fracture provided that the proppant size is homogeneous, and the fracture width is equal to one proppant diameter. Placing more proppant particles in the fracture will not help increase the fracture width because there is no proppant embedment. Instead, the increasing number of proppant particles in the fracture blocks the pore space, leading to reduced fracture porosity, permeability, and consequently fracture conductivity. In reality, however, using only one proppant particle in the fracture is never the optimal solution because the compressive effective stress results in proppant embedment, as we observed in this experimental study. This, again, emphasizes that it is critical to account for proppant embedment on rock surfaces when studying fracture conductivity under various proppant concentrations and effective stresses.

5. Conclusions and implications

This is the first study that used well-controlled laboratory experiments to comprehensively investigate non-monotonic fracture conductivity evolution as a function of increasing proppant concentration under various effective stresses, proppant particle sizes, rock types, and water soaking time. With seven proppant concentrations (up to 2 lb/ft^2) and seven effective stresses (up to 6000 psi) used in the conductivity measurements, we experimentally confirmed that the correlation between fracture conductivity and proppant concentration was non-monotonic because of a competing process between fracture permeably and fracture width. A relatively good agreement was observed between the laboratory-measured and our previous model-derived fracture-conductivity versus proppant-concentration curves. We also investigated the influences of effective stress, proppant particle diameter, rock type, and water soaking on the OPPC and OFC. The effective stress had a more significant impact on the OFC than on the OPPC.

The existence of the OPPC indicates that a relatively low proppant amount can be used to form a partial-monolayer proppant pack in the fracture space, which has similar or higher fracture conductivity compared to a multilayer proppant assembly structure. This finding has important economic implications because high-strength, ultralight-weight proppant particles can be used to form partial-monolayer proppant packs in fractures, leading to sufficiently high fracture conductivity using a much lower material cost compared to multilayer proppant structures.

Proppant embedment is the primary mechanism that causes the competing process between fracture width and fracture permeability and consequently the non-monotonic fracture conductivity evolution as a function of increasing proppant concentration. Without proppant embedment, there will not be such a competing process, and we will not observe the non-monotonic fracture conductivity evolution. Some numerical studies in the literature, for the sake of simplicity, assumed that the proppant particles and rock surfaces are ideal, rigid materials, which means that proppant embedment on rock surfaces does not occur. Based on this no-embedment assumption, the simulated fracture conductivity decreased monotonically with an increasing proppant concentration when the proppant assembly is a partial-monolayer structure. In other words, the OPPC in this case is to place only one proppant particle in the fracture because it provides the highest fracture porosity and permeability. In reality, however, using only one proppant particle in the fracture is never the optimal solution because the compressive stress results in proppant embedment. This, again, emphasizes that it is critical to account for proppant embedment on rock surfaces when studying fracture conductivity under various proppant concentrations and effective stresses.
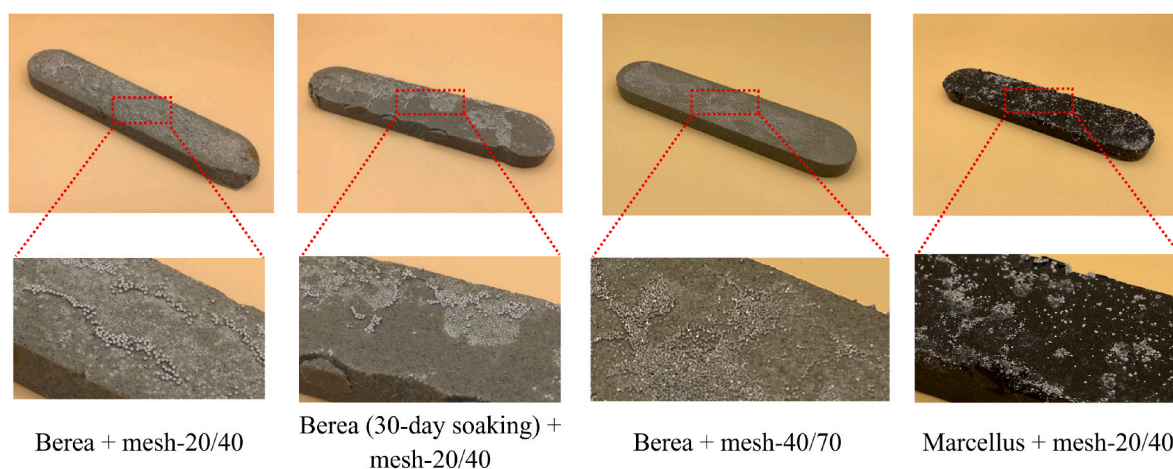

| Berea + mesh-20/40 | Berea (30-day soaking) + mesh-20/40 | Berea + mesh-40/70 | Marcellus + mesh-20/40 |

Fig. 8. Rock slab surfaces after the 6000 psi testing with a ceramic proppant concentration of 0.06 lb/ft^2.
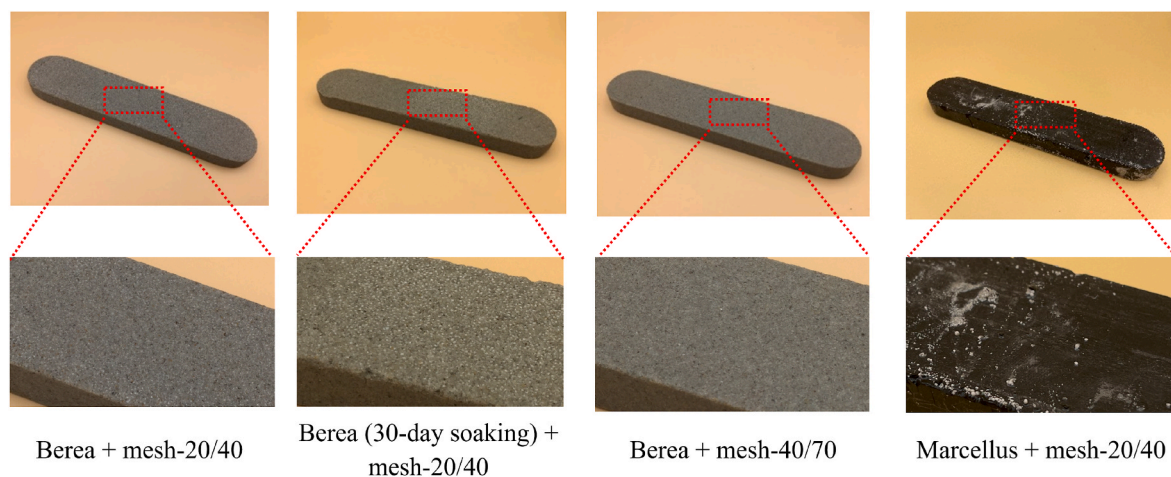
Fig. 9. Rock slab surfaces after the 6000 psi testing with a ceramic proppant concentration of 2 lb/ft^2.

Author contributions

Zihao Li: conceptualization, methodology, conducting experiment, result analysis, writing and editing original manuscript. **Qingqi Zhao**: methodology, conducting experiment, and writing original manuscript. **Yuntian Teng**: methodology and conducting experiment. **Nino Ripepi**: conceptualization and methodology. **Ming Fan**: methodology and result analysis. **Xiaolong Yin**: conceptualization and methodology. **Cheng Chen**: conceptualization, methodology, supervision, result analysis, writing review and editing original manuscript.

Declaration of competing interest

The authors declare that they have no known competing financial interests or personal relationships that could have appeared to influence the work reported in this paper.

Acknowledgments

References

Bestaoui-Spurr, N., Hudson, H., 2017. Ultra-Light Weight Proppant and Pumping Design Lead to Greater Conductive Fracture Area in Unconventional Reservoirs. Society of Petroleum Engineers. https://doi.org/10.2118/185435-MS.

Bhandakkar, P., Siddhamshetty, P., Kwon, J.S.I., 2020. Numerical study of the effect of propped surface area and fracture conductivity on shale gas production: application for multi-size proppant pumping schedule design. J. Nat. Gas Sci. Eng. 79, 103349.

Brannon, H.D., Malone, M.R., Rickards, A.R., et al., 2004. Maximizing fracture conductivity with proppant partial monolayers: theoretical curiosity or highly productive reality?. In: SPE Annual Technical Conference and Exhibition. Society of Petroleum Engineers, Houston, Texas, September. https://doi.org/10.2118/90698-MS. SPE-90698-MS.

Chen, C., Packman, A.I., Gaillard, J.F., 2008. Pore-scale Analysis of permeability reduction resulting from colloid deposition. Geophys. Res. Lett. 35 (7), L07404. https://doi.org/10.1029/2007GL033077.

Chen, C., Lau, B.L.T., Gaillard, J.F., et al., 2009. Temporal evolution of pore geometry, fluid flow, and solute transport resulting from colloid deposition. Water Resour. Res. 45 (6), W06416. https://doi.org/10.1029/2008WR007252.

Chen, C., Martysevich, Vl, O'Connell, P., et al., 2015. Temporal evolution of the geometrical and transport properties of a fracture/proppant system under increasing effective stress. SPE J. 20 (3), 527–535. https://doi.org/10.2118/171572-PA. SPE-171572-PA.

Dahl, J., Nguyen, P., Dusterhoft, R., et al., 2015. Application of micro-proppant to enhance well production in unconventional reservoirs: laboratory and field results. In: SPE Western Regional Meeting. https://doi.org/10.2118/174060-MS. Garden Grove, California, April. SPE-174060-MS.

Darin, S.R., Huitt, J.L., 1960. Effect of a partial monolayer of propping agent on fracture flow capacity. Society of Petroleum Engineers 219 (1), 31–37. https://doi.org/10.2118/1291-G. SPE 1291-G.

Economides, M.J., Nolte, K.G., 2000. Reservoir Stimulation, third ed. John Wiley and Sons.

Fan, M., McClure, J., Han, Y., et al., 2019. Using an experiment/simulation-integrated approach to investigate fracture-conductivity evolution and non-Darcy flow in a proppant-supported hydraulic fracture. SPE J. 24 (4), 1912–1928. https://doi.org/10.2118/195588-PA. SPE-195588-PA.

Fan, M., Li, Z., Han, Y., et al., 2021. Experimental and numerical investigations of the role of proppant embedment on fracture conductivity in narrow fractures. SPE J. 26 (1), 324–341. https://doi.org/10.2118/204222-PA. SPE-204222-PA.

Gaurav, A., Dao, E.K., Mohanty, K.K., 2012. Evaluation of ultra-light-weight proppants for shale fracturing. J. Petrol. Sci. Eng. 92, 82–88. https://doi.org/10.1016/j.petrol.2012.06.010.

Gensterblum, Y., Ghanizadeh, A., Cuss, R.J., et al., 2015. Gas transport and storage capacity in shale gas reservoirs–A review. Part A: transport processes. J. Unconv. Oil Gas Resour. 12, 87–122. https://doi.org/10.1016/j.juogr.2015.08.001.

Gu, M., Dao, E., Mohanty, K.K., 2015. Investigation of ultra-light weight proppant application in shale fracturing. Fuel 150, 191–201. https://doi.org/10.1016/j.fuel.2015.02.019.

Hu, T., Pang, X., Jiang, F., et al., 2021. Movable oil content evaluation of lacustrine organic-rich shales: methods and a novel quantitative evaluation model. Earth Sci. Rev. 214, 103545. https://doi.org/10.1016/j.earscirev.2021.103545.

Huitt, J.L., Mcglothlin, B.B., 1958. The Propping of Fractures in Formations Susceptible to Propping-Sand Embedment. Drilling and Production Practice. American Petroleum Institute, New York, New York. January. API-58-115. Retrieved from. https://onepetro.org/APIDPP/proceedings-abstract/API58/All-API58/API-58-115/51121.

Kunnath Aven, N., Weaver, J., Loghry, R., et al., 2013. Long-term dynamic flow testing of proppants and effect of coatings. In: SPE European Formation Damage Conference & Exhibition. Society of Petroleum Engineers. https://doi.org/10.2118/165118-MS. Noordwijk, The Netherlands, June. SPE-165118-MS.

Li, Z., Zhang, W., Tang, Y., et al., 2016. Formation damage during alkaline-surfactant-polymer flooding in the sanan-5 block of the daqing oilfield, China. J. Nat. Gas Sci. Eng. 35, 826–835. https://doi.org/10.1016/j.jngse.2016.07.046.

Li, Z., Ripepi, N., Chen, C., 2019. August. Comprehensive laboratory investigation and model fitting of klinkenberg effect and its role on apparent permeability in various US shale formations. In: 53rd U.S. Rock Mechanics/Geomechanics Symposium. New York City, New York, June. ARMA-2019-1568. Retrieved from. https://onepetro.org/ARMAUSRMS/proceedings-abstract/ARMA19/All-ARMA19/ARMA-2019-1568/124915.

Li, Z., Ripepi, N., Chen, C., 2020. Using pressure pulse decay experiments and a novel multi-physics shale transport model to study the role of klinkenberg effect and effective stress on the apparent permeability of shales. J. Petrol. Sci. Eng. 189, 107010. https://doi.org/10.1016/j.petrol.2020.107010.

Li, C., Lin, M., Liu, J., et al., 2021. The probability of oil and water movement in tight sandstone: evaluation methodology and mechanism analysis. J. Petrol. Sci. Eng. 196, 107661. https://doi.org/10.1016/j.petrol.2020.107661.

Liang, F., Sayed, M., Al-Muntasheri, G.A., et al., 2016. A comprehensive review on proppant technologies. Petroleum 2 (1), 26–39. https://doi.org/10.1016/j.petlm.2015.11.001.

McGinley, M., Zhu, D., Hill, A.D., 2015. The effects of fracture orientation and elastic property anisotropy on hydraulic fracture conductivity in the Marcellus Shale. In: SPE Annual Technical Conference and Exhibition. https://doi.org/10.2118/174870-MS. Houston, Texas, September. SPE-174870-MS.

Mittal, A., Rai, C.S., Sondergeld, C.H., 2018. Proppant-conductivity testing under simulated reservoir conditions: impact of crushing, embedment, and diagenesis on long-term production in shales. SPE J. 23 (4), 1304–1315. https://doi.org/10.2118/191124-PA. SPE-191124-PA.

Montgomery, C.T., Smith, M.B., 2010. Hydraulic fracturing: history of an enduring Technology. J. Petrol. Technol. 62 (12), 26–40. https://doi.org/10.2118/1210-0026-JPT. SPE-1210-0026-JPT.

Parker, M.A., Ramurthy, K., Sanchez, P.W., 2012. New proppant for hydraulic fracturing improves well performance and decreases environmental impact of hydraulic fracturing operations. In: SPE Eastern Regional Meeting. Lexington, Kentucky. https://doi.org/10.2118/161344-MS. October. SPE-161344-MS.

Posey, D.B., Strickland, B.D., 2005. The effect of using a lightweight proppant in treatment of a low-permeability, dry-gas reservoir: a case study. In: The SPE Eastern Regional Meeting. https://doi.org/10.2118/97998-MS. Morgantown, West Virginia, September. SPE-97998-MS.

Raysoni, N., Weaver, J., 2013. Long-term hydrothermal proppant performance. SPE Prod. Oper. 28 (4), 414–426. https://doi.org/10.2118/150669-PA. SPE-150669-PA.

API RP-19D, 2008. Measuring the Long-Term Conductivity of Proppants. API, Washington, DC, USA.

Tan, X., Gilliland, E., Tang, X., et al., 2020. Integrated experimental characterization of shales of varying thermal maturation in the central appalachian basin using Raman and fourier transform infrared spectroscopy and atomic force microscopy. Energy Fuels 35 (1), 201–212. https://doi.org/10.1021/acs.energyfuels.0c01836.

Tillman, D.A., Warshauer, J.B., Prinzing, D.E., by Staff, U., 2015. Fuel resources. In: Kirk-Othmer Encyclopedia of Chemical Technology, (Ed.). John Wiley & Sons, Inc. https://doi.org/10.1002/0471238961.0621051220091212.a01.pub2.

Wang, H., Rabiei, M., Wang, S., et al., 2018. Fracture quantification method with 3D X-ray image-entropy-assisted indicator kriging method. In: The SPE Western Regional Meeting. https://doi.org/10.2118/190045-MS. Garden Grove, California, April. SPE-190045-MS.

Weaver, J.D., Rickman, R.D., Luo, H., et al., 2009. A study of proppant formation reactions. In: SPE International Symposium on Oilfield Chemistry. https://doi.org/10.2118/121465-MS. Woodlands. Texas, April. SPE-121465-MS.

Zhang, J., Zhu, D., Hill, A.D., 2016. Water-induced damage to propped-fracture conductivity in shale formations. SPE Prod. Oper. 31 (2), 147–156. https://doi.org/10.2118/173346-PA. SPE-173346-PA.

Zhang, F., Zhu, H., Zhou, H., et al., 2017. Discrete-element-method/computational-fluid-dynamics coupling simulation of proppant embedment and fracture conductivity after hydraulic fracturing. SPE J. 22 (2), 632–644. https://doi.org/10.2118/185172-PA. SPE-185172-PA.

Zhao, Q., Zhu, J., Cao, G., et al., 2021. Transient modeling of plunger lift for gas well deliquification. SPE J. 1–20 https://doi.org/10.2118/205386-PA. SPE-205386-PA.

Zheng, W., Silva, S.C., Tannant, D.D., 2018. Crushing characteristics of four different proppants and implications for fracture conductivity. J. Nat. Gas Sci. Eng. 53, 125–138. https://doi.org/10.1016/j.jngse.2018.02.028.